

Article

Effects of Laser Operating Parameters on Piezoelectric Substrates Micromachining with Picosecond Laser

Lamia EL Fissi *, Victor Xhurdebise and Laurent A. Francis

Institute of Information and Communication Technologies, Electronics and Applied Mathematics (ICTEAM), Université Catholique de Louvain, B-1348 Louvain-la-Neuve, Belgium;
E-Mails: victorxhurdebise@gmail.com (V.X.); laurent.francis@uclouvain.be (L.A.F.)

* Author to whom correspondence should be addressed; E-Mail: lamia.elfissi@uclouvain.be;
Tel.: +32-1047-2174; Fax: +32-1047-2598.

Academic Editor: Maria Farsari

Received: 18 July 2014 / Accepted: 8 December 2014 / Published: 23 December 2014

Abstract: Ten picoseconds (200 kHz) ultrafast laser micro-structuring of piezoelectric substrates including AT-cut quartz, Lithium Niobate and Lithium Tantalate have been studied for the purpose of piezoelectric devices application ranging from surface acoustic wave devices, e.g., bandpass filters, to photonic devices such as optical waveguides and holograms. The study examines the impact of changing several laser parameters on the resulting microstructural shapes and morphology. The micromachining rate has been observed to be strongly dependent on the operating parameters, such as the pulse fluence, the scan speed and the scan number. The results specifically indicate that ablation at low fluence and low speed scan tends to form a U-shaped cross-section, while a V-shaped profile can be obtained by using a high fluence and a high scan speed. The evolution of surface morphology revealed that laser pulses overlap in a range around 93% for both Lithium Niobate (LiNbO₃) and Lithium Tantalate (LiTaO₃) and 98% for AT-cut quartz can help to achieve optimal residual surface roughness.

Keywords: picosecond; piezoelectric substrates; AT-cut quartz; Lithium Niobate; Lithium Tantalate; fluence; scan speed; scan number; laser ablation

1. Introduction

Transparent materials are particularly interesting for microsystems technology. They can be passive materials or active materials, like piezoelectric quartz crystals, as well as piezoelectric and electro-optic/acoustic Lithium Niobate and Lithium Tantalate for actuators and sensors. In general, transparent materials display excellent properties, such as a high transmission from ultraviolet (UV) to infrared (IR) light, a high hardness, excellent thermal properties, a high electrical insulation, and a high thermal and chemical stability. However, it is difficult to etch well-defined structures on such substrates especially to obtain crack-free structures [1–3].

The laser processing of transparent materials has been studied extensively [4–6]. The laser ablation has a number of advantages for micromachining: it is a single-step process with a high flexibility, a direct patterning without a photosensitive resist process, and high etching rates which allow fast prototyping. A variety of lasers can be used for micromachining, from nanosecond lasers to ultrafast lasers, or from IR lasers to UV lasers, depending on the materials to be processed and the desired applications [7–14]. The transparent material machining with long pulse lasers (pulses longer than the electron-phonon relaxation time) has been very challenging as the laser-induced thermal stresses often leads to micro-cracks. Redeposition of molten material on machined surfaces can be difficult to remove, which significantly reduces the surface quality. With advancement of short lasers, surface as well as sub-surface machining has been the focus of many studies recently [15–19]. Both picosecond and femtosecond pulses have been demonstrated to be very efficient for high-precision material processes with sharp edges and limiting the heat affected zone.

During ultrashort pulse lasers (less than 10 ps), the light is absorbed by the electrons and increases rapidly their energy which may cause nonlinear effects or direct emission of electrons. The material is heated with delay in the order of the electron-phonon relaxation time. This time is material-dependent on the time scale of 0.1–20 ps [20–24]. Electron-phonon coupling is a driving force in redistribution of absorbed energy, and response of the material might be affected by excitation. Therefore, for a given set of laser parameters, e.g., fluence and wavelength, the pulse duration has a significant effect on micromachining results [25,26]. The laser radiation with the pulse duration shorter than the characteristic time is desirable for processing with the minimal thermal load to the material. On the other hand, precision of ultra-short laser fabrication is tightly related to the removal of material in small portions. The use of pulses with the duration of a few nanoseconds is well balanced in some cases between the high removal rate, with long pulses, and high quality of ultra-short-pulse fabrication [23].

In this paper, we investigated the ultraviolet picosecond laser-induced microstructures via direct writing on the surface of non-conventional materials. The study focuses on piezoelectric substrates including AT-cut quartz (ALPHA-SiO₂), Lithium Niobate (LiNbO₃) and Lithium Tantalate (LiTaO₃) (The most used materials for surface acoustic wave sensors). The study examines the ablation efficiency and the impact of changing several laser operating parameters (scan number, scan speed, and pulse fluence) on the resulting microstructural shapes. The evolution of surface morphology, the residual surface roughness, and the ablation rate under varying conditions are studied and reported.

2. Experimental Section

Figure 1 presents the schematic illustration of the experimental setup. The experiments were performed using Coherent Talisker DPSS (Oxford Lasers, Shirley, NY USA) picosecond laser emitting at 355 nm from Oxford Lasers. The typical pulse duration is 10 ps. The pulse repetition rate was set up to 200 kHz and the average laser power to 3 W. The laser beam was scanned over the sample using an optical 2D deflection unit with an integrated focusing unit. The sample was mounted on a *XY* table, while galvo mirrors were used to control the beam displacement. The UV focal spot diameter is 10 μm. In order to guarantee high machining quality, the focus distance must be readjusted according to each sample thickness to preserve a focalized beam on the sample surface and thus a perpendicular contact between the beam and the sample.

To determine the effects of laser operating parameters on resulting microstructural shapes and morphology, the desired pattern (rectangular areas of 1 by 1 mm² with separated by 1 mm and grooves areas of 0.05 by 1 mm² with separated by 0.05 mm) is applied to the substrates by writing adjacent lines with varying laser parameters. The ranges of the operating parameters, including scanning speed, scan number, and pulse fluence are listed in Table 1.

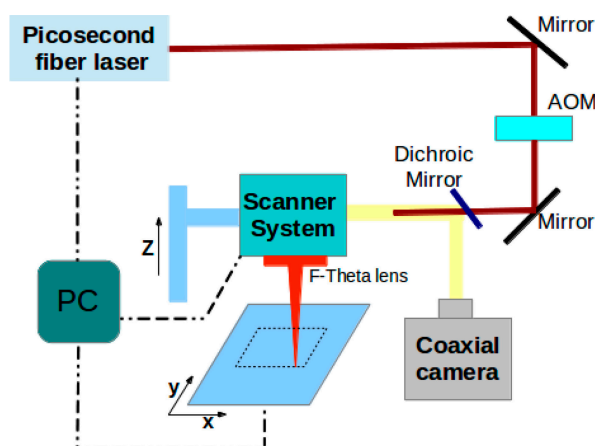


Figure 1. Schematic illustration of the experimental setup.

Table 1. Operating parameters of laser ablation.

Parameter (units)	Values
Scan speed (mm·s ⁻¹)	5, 10, 20, 30, 40, 50
Scan number	1, 2, 3, 4, 5, 6, 7, 8, 9, 10
Fluence (J·cm ⁻²)	0.62, 0.93, 1.24, 1.55, 1.86, 2.17, 2.48, 2.79, 3.1
Repetition rate (kHz)	33

After the laser ablation, the debris is often accumulated on the machined surface and has to be discarded, so that it does not erroneously affect sample analysis or measurements. A mixture of 49% HF and 69% HNO₃ solution (Buffered Hydrofluoric acid (BHF)) in the ratio of 5:1 solution can effectively clean the debris. As we can see in Figure 2, after 10 s in BHF solution the surface roughness of 1 mm² rectangle is decreased by 100 nm, independently of the material, compared with surface roughness of substrate without BHF. After 10 s, surface roughness increases linearly with increasing the time in the BHF solution. We can conclude that 10 s is enough to remove the debris

without etching the machined surface. Surface morphologies of ablated materials were measured at the bottom of rectangles by using an interferometer (Polytech MSA 500 Micro System Analyzer, Polytec, Irvine, CA, USA). For the rest of the study, all micromachined structures were cleaned by BHF solution for 10 s and then characterized.

The materials considered are AT-cut quartz single crystal, X-cut LiNbO₃ single crystal, and Y-cut LiTaO₃. All of them are a single side polished (500 μm thick) and bought from Roditi International Corporation Ltd. (London, UK.) The optical properties of these materials are presented in Table 2.

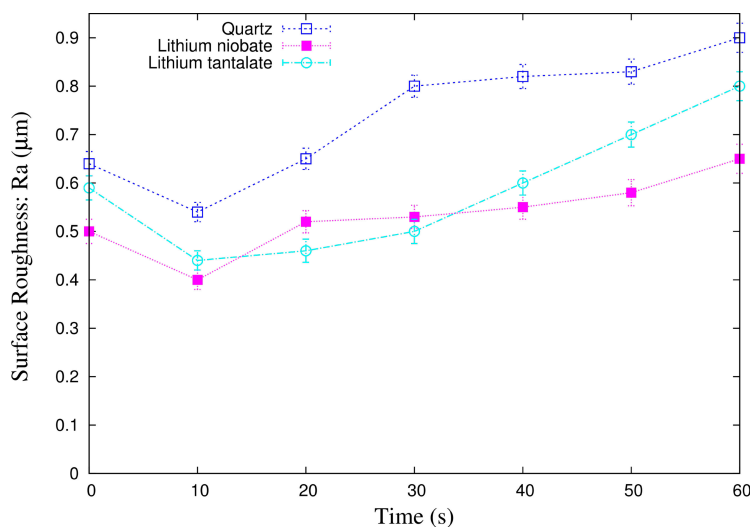


Figure 2. Effect of BHF solution on the surface roughness; $F = 0.55 \text{ J}\cdot\text{cm}^{-2}$, Scan number = 6. Each data point shows the average and standard deviation from 10 measurements.

Table 2. Thermophysical properties of AT-cut quartz, LiNbO₃, and LiTaO₃ [27,28].

Properties (units)	AT-cut quartz	LiNbO ₃	LiTaO ₃
Density (kg/m ³)	2684	4640	7450
Heat Capacity (J/K/mol)	741	89	100
Thermal conductivity (W/m/K)	3.2	5.6	4.6
Melting point (°C)	1740	1350	1605
Transmittance Range (nm)	400–3500	350–5000	400–5000

The laser machined microstructures were observed with a Nikon optical microscope with CCD camera. Ablated deep material was determined by using an optical surface profiling (DEKTAK 150 Profilometer, Veeco, Plainview, NY, USA). A conventional Scanning Electron Microscope (SEM) (Leo Ultra 55 FEG SEM, Zeiss, Oberkochen, Germany) was also used to inspect the microstructural shapes at higher magnifications.

3. Results and Discussion

3.1. Effects of Scan Number and Scan Speed

The effects of the scan speed and the scan number on the etch rate (ablation depth) and the surface roughness of the three materials are studied in this section. The scan number is defined as the number of times that the laser beam scans the rectangle surface (1 mm²). Six scan speeds are considered (see

Table 1). The repetition rate and the fluence are fixed at 33 kHz and $0.55 \text{ J}\cdot\text{cm}^{-2}$, respectively. The relationships between the ablation depth, surface roughness, and the scan number for the six scan speeds are plotted in Figure 3. Each data point shows the average and the standard deviation from 10 measurements. From the data shown in Figure 3a,c,e, the linear fitting indicated that the ablation depth is essentially proportional to the scan number independently of the scan speed. We believed that the linearity is resulted from the vaporized material that has left the cavity without redeposition. Note that the increment of input energy is linearly proportional to the increment of scan number and that this statement is correct for the range of the parameters presented in the Table 1. As the focus was not changed during the etching, the effective fluence decreases with the number of scans and the ablation rate should start decreasing (this regime is not visible in Figure 3).

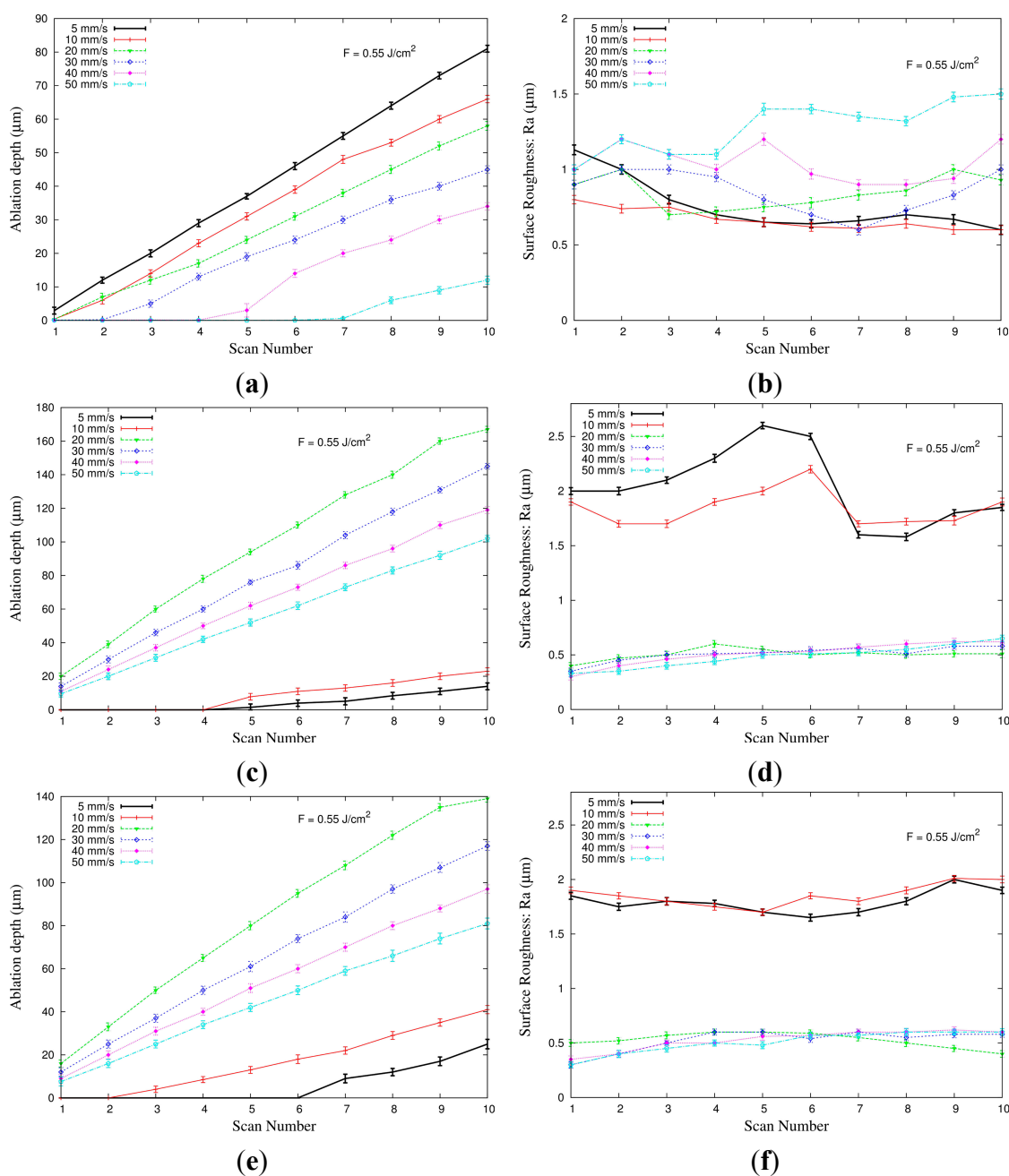


Figure 3. Effect of scan number on the ablation depth and surface roughness at a fluence of $0.55 \text{ J}\cdot\text{cm}^{-2}$. (a,b) AT-cut quartz, (c,d) LiNbO₃, (e,f) LiTaO₃.

The scanning speed had a great impact on ablation process efficiency of the three materials. As shown in Figures 3 and 4, the etch rate of AT-cut quartz is less than LiNbO₃ and LiTaO₃ for a scan speed higher than 20 mm·s⁻¹. For LiNbO₃ and LiTaO₃, the highest etch rate is observed for the scan speed equal to 20 mm·s⁻¹ while residual surface roughness is nearly constant at 500 nm (also for scan speed higher than 20 mm·s⁻¹). However, for AT-cut quartz the highest etch rate is seen for 5 mm·s⁻¹ while residual surface roughness is nearly at 550 nm for the scan speed lower than 10 mm·s⁻¹.

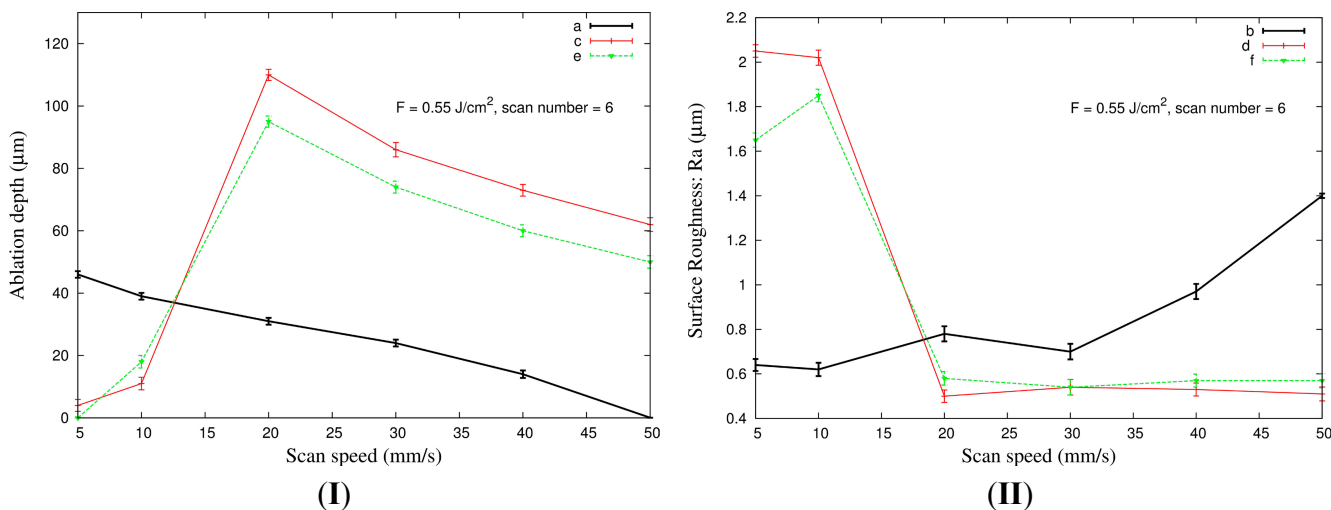


Figure 4. Effect of scan speed (I) on the ablation depth and surface roughness (II) at a fluence of 0.55 J·cm⁻². (a,b) AT-cut quartz, (c,d) LiNbO₃, (e,f) LiTaO₃.

For a given material, the ablation threshold can depend on the presence of defects in the material [29]. These defects can be created by the exposition to laser pulses, with fluences lower than the ablation threshold for one pulse. So when overlapping pulses, there can be no ablation but generation of defects in the material (change of the mechanical/chemical properties) which are lowering the ablation threshold. This effect is called incubation effect [30]. The incubation can explain why, as visible on Figure 3, for AT-cut quartz at speeds higher than 40 mm·s⁻¹, there is no ablation before a certain number of scans.

Since the threshold values of AT-cut quartz, LiNbO₃ and LiTaO₃ are relatively high, the ablations of these materials are primarily a thermal or photothermal process. The photothermal process dominates for ablation of ceramics and metals which possess high thresholds [31,32]. In a photothermal process the absorbed laser energy is converted to lattice vibrational energy (thermal) to melt and vaporize the material. To directly break atomic bonding, the intensity of the laser beam should be higher than a threshold value, which is mainly dependent on the material to be ablated and the wavelength of the laser. At intensities below the ablation threshold, the absorbed energy heats the substrate and raises the substrate temperature higher than its boiling or sublimation point and as a result the material begins to liberate.

Consequently, their associated thermal properties are important in the interpretation of their ablation results. Based on the material properties shown in Table 2, the melting temperature of AT-cut quartz is relatively high (1740 °C) as compared to LiNbO₃ and LiTaO₃ (1350 and 1605 °C, respectively), and its thermal conductivity (3.2 W/m·K) is lower than the both (5.6 and 4.6 W/m·K, respectively). Thus,

the heat converted by laser energy does not accumulate fast enough to melt AT-cut quartz when increasing the scan speed. Consequently, the etch rate of AT-cut quartz is smaller than the LiNbO₃ and LiTaO₃ for a scan speeds higher than 20 mm·s⁻¹. Compared between LiNbO₃ and LiTaO₃, the thermal conductivity of LiTaO₃ is lower than LiNbO₃, but it has a higher melting temperature. The combination of these two properties makes Lithium tantalate's etch rate 20% less than the etch rate of LiNbO₃.

For ultrashort pulse laser micromachining, the pulse overlap is crucial to obtain depth structures with low surface roughness [33]. The pulse overlap is calculated from the following relation:

$$OP = 1 - \frac{v}{2\omega_0 f}$$

where v is the scan speed, $2\omega_0$ is the focused spot diameter and f is the laser repetition rate. In our case: $f = 33$ kHz; $2\omega_0 = 10$ μm. According to data shown in Figure 3, the optimized pulse overlap for AT-cut quartz is observed at 98%, while for LiNbO₃ and LiTaO₃ it is seen at 93%.

3.2. Effect of Fluence

The relationships between the ablation depth, the surface roughness, and the laser fluence for two scan speeds are plotted in Figure 5. The fluence is estimated from the measured pulse energy and the focal spot diameter. The scan number is fixed arbitrarily at 5 (number of times that the laser beam scans rectangle surface (0.16 mm × 1 mm)). Each data point shows the average and standard deviation from 10 measurements. The material removal rate was strongly related to the fluence. Once the ablation threshold was exceeded the material removal efficiency began to increase with increasing fluence. The threshold for each material was determined experimentally by measuring the etch rates at various laser fluences (shown in Figure 5a,c,e). The threshold fluence of At-cut quartz for irradiation at 355 nm is 1.3 J·cm⁻². As can be seen from the data presented in Figure 5a,c,e), two behaviors were observed depending on scan speed:

For AT-cut quartz with low scan speed (5 mm·s⁻¹), the laser induced temperature increase at low fluences (below 1.2 J·cm⁻²) does probably not reach the melting point of quartz (the threshold fluence is about 1.3 J·cm⁻²). However, after this value the etch rate is proportional to the fluence. In the case of LiNbO₃ and LiTaO₃ a sweet spot is found, at which the ablation efficiency reaches its maximum. Above this optimum fluence the efficiency decreases strongly. At low fluences (below 1.8 J·cm⁻²) the etch rate increases linearly with fluences. For higher fluence (starting around 1.8 J·cm⁻²), the etching is significantly inhomogeneous across the rectangles. Un-etched material remains in the center of the rectangles (Figure 6) and tends to be larger in volume as the writing energy increases (Figure 5c,e). There is a reasonable explication for the ablation decrease. The machined depth and removed volume depend mainly on the amount of energy deposited on the substrate.

At low scan speed with a high fluence, laser beam removes a bigger volume of LiNbO₃ and LiTaO₃ and with a repetition rate of 33 kHz time is insufficient to sputtered the debris removed which can be cooled down and solidified in the rectangle micromachined (Figure 6).

For high scan speed (20 mm·s⁻¹), the variation in the etch rate as a function of the applied laser pulse fluence can be distinguished by two different interaction regimes: one is the initial approximate linear increase regime of the etch rate at low fluence, and the other is the trend of the partial or complete saturation regime at a relatively high fluence.

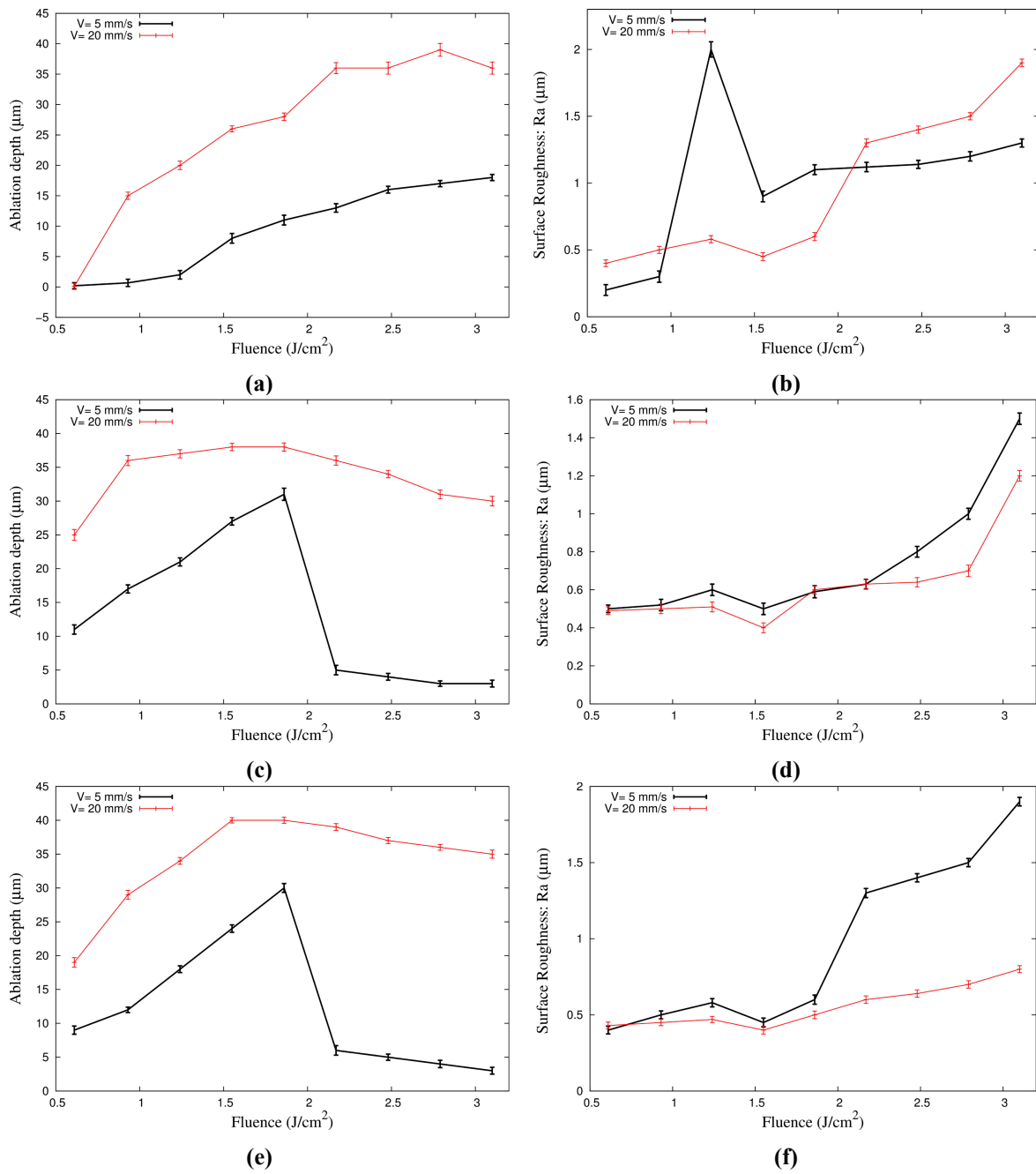


Figure 5. Effect of fluence on the ablation depth and surface roughness (scan number = 5) for (a,b) AT-cut quartz, (c,d) LiNbO₃, and (e,f) LiTaO₃.

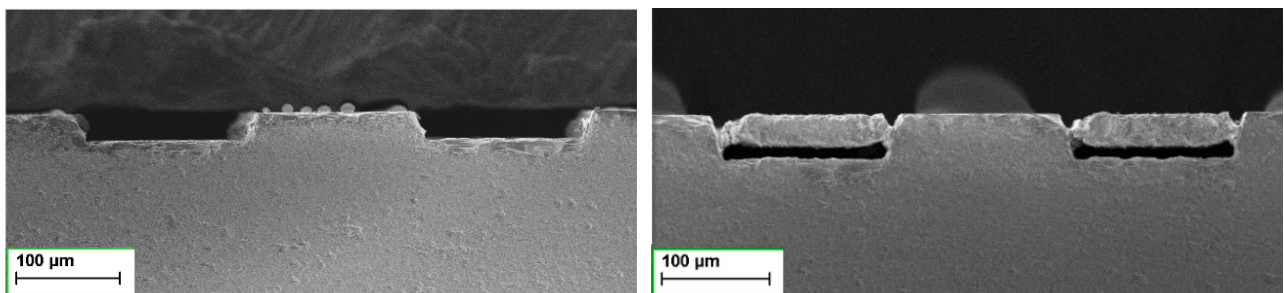


Figure 6. SEM pictures of LiNbO₃ micromachining surface ($0.16\text{ mm} \times 1\text{ mm}$) at: $V = 5\text{ mm}\cdot\text{s}^{-1}$ and $f = 33\text{ kHz}$ (left) at $F = 1.55\text{ J}\cdot\text{cm}^{-2}$ (right) at $F = 2.79\text{ J}\cdot\text{cm}^{-2}$.

After the material surface has absorbed the laser energy, the material will heat, melt, vaporize, and splash so that a variety of mechanisms can generate the phenomena of mass migration, erosions or loss with the linear and non-linear processes [34,35]. With the increase in the laser fluence, the accumulation of photon energy increases, and the number of free electrons with high temperature from the photons absorbed by multi-photon ionization will also increase. In this manner, material removal will be more important and the etch rate will increase. The saturation regime may arise from the development of the free carrier plasma. Free electrons with high temperature will be produced instantaneously under laser irradiation, the high temperature will transfer heat to the lattice through thermal conductivity, and the bound electron will be stripped of atoms to produce high density plasma with high temperature and high pressure. Then the plasma will quickly break away from the parent material surface in the form of spatter by Coulomb repulsion to achieve the material ablation. With relatively high fluence, the plasma generation is greater. When the plasma density accumulates to a certain critical value, the coulomb repulsion of the interaction with plasma will be difficult to splash out completely, and the plasma becomes highly absorbing, which will create a partial plasma deposit and remain on the material's surface. Then the plasma density generation under high fluence will exceed the critical value and the deposited plasma will gradually make the etch rate tend towards saturation. Figure 5b,d,f illustrates the machined surface roughness changing with fluence. It reveals an increase of surface roughness with increasing the fluence independently of the scan speed. Compared between the three types of materials, AT-cut quartz presents the highest surface roughness. However, the etching at the fluence $1.55 \text{ J}\cdot\text{cm}^{-2}$ presents the best surface roughness independently of the type of material.

3.3. Ablation Trench Shapes

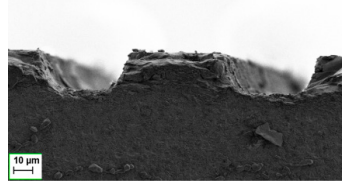
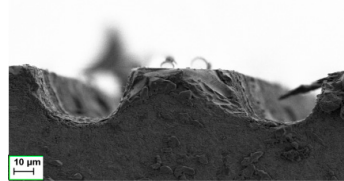
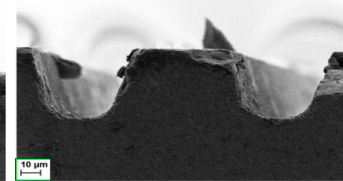
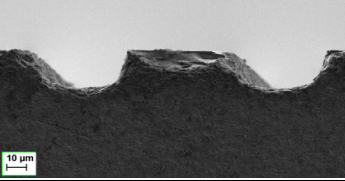
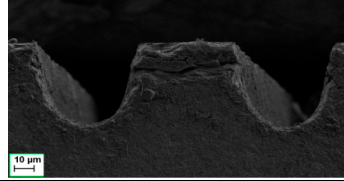
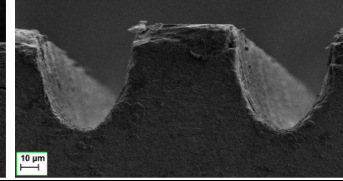
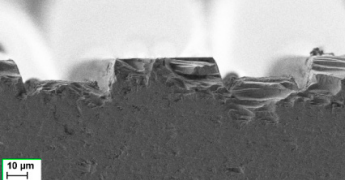
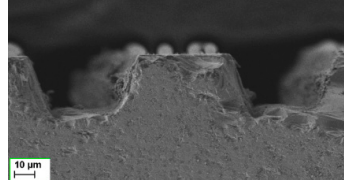
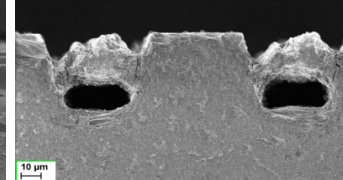
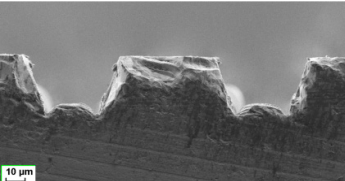
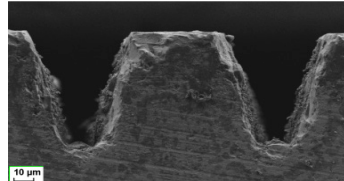
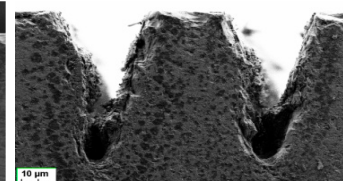
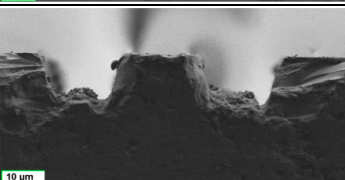
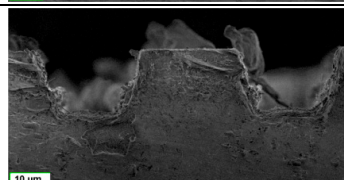
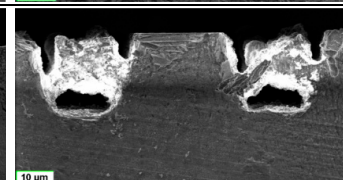
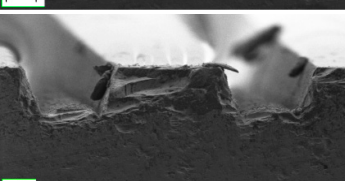
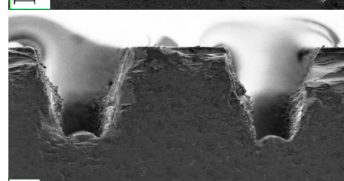
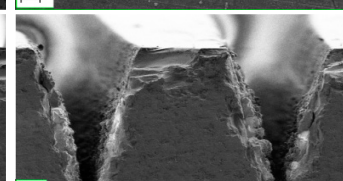
Laser beam strikes a target; the target material is rapidly melted and partially vaporized. In ceramics, the photothermal effect is dominant. If the vaporized elements are continuously bombarded by the subsequent laser beams, their temperatures keep rising and the vaporized elements eventually ionize to plasma. The ionized vapor or plasma can continuously absorb the rest of laser energy and rapidly expand outward, forming plasma pressure waves [30]. The lifetime or duration of plasma state is very short, on the order of pico/femtoseconds [36], and the plasma waves will not interact with those of subsequent laser pulses because the repetition rate: Concurrently, this high vapor- and ion- pressure build-up can sputter away melted materials to form fine droplets, resulting in small cavities in the target material. The forming of small cavities and sputtering droplets is a major material-removing mechanism in laser ablation.

Rectangular patterns (0.05 by 1 mm^2) were made by scanning adjacent lines at a repetition rate of 33 kHz and five scan numbers. Two different scan speeds (5 and $20 \text{ mm}\cdot\text{s}^{-1}$) and three different fluences (0.61 , 1.55 , and $3.1 \text{ J}\cdot\text{cm}^{-2}$) were considered. The three substrates were cleaned after ablation for 10 s using a BHF solution. The relationship between the ablation trench shapes and fluences are presented in Table 3.

As we can see from Table 3, low fluence ($0.61 \text{ J}\cdot\text{cm}^{-2}$) does not affect the ablation shape of the different substrates much while scan speed affects trench shape. As the fluence increases the trench shapes change. For AT-cut quartz, the cross sectional profile produced by high fluence ($1.55 \text{ J}\cdot\text{cm}^{-2}$

and $3.1 \text{ J}\cdot\text{cm}^{-2}$) is U-shaped for low scan speed ($5 \text{ mm}\cdot\text{s}^{-1}$) and the one produced by high scan speed ($20 \text{ mm}\cdot\text{s}^{-1}$) becomes oval shaped. Concerning LiNbO_3 and LiTaO_3 , the U-shaped is also observed for low scan speed and at $F = 1.55 \text{ J}\cdot\text{cm}^{-2}$. For high fluence (between 2.45 and $3.1 \text{ J}\cdot\text{cm}^{-2}$) inhomogeneous shape is observed (un-etched material remains in the center of the rectangles). The V-shaped is observed for both materials for high scan speed ($20 \text{ mm}\cdot\text{s}^{-1}$) at high fluence.

Table 3. Effect of fluence on ablation shape of AT-cut quartz, LiNbO_3 and LiTaO_3 at two scan speeds (5 and $20 \text{ mm}\cdot\text{s}^{-1}$).

Shape	Scan speeds	$0.61 \text{ J}\cdot\text{cm}^{-2}$	$1.55 \text{ J}\cdot\text{cm}^{-2}$	$3.1 \text{ J}\cdot\text{cm}^{-2}$
AT-cut quartz	$5 \text{ mm}\cdot\text{s}^{-1}$			
	$20 \text{ mm}\cdot\text{s}^{-1}$			
LiNbO_3	$5 \text{ mm}\cdot\text{s}^{-1}$			
	$20 \text{ mm}\cdot\text{s}^{-1}$			
LiTaO_3	$5 \text{ mm}\cdot\text{s}^{-1}$			
	$20 \text{ mm}\cdot\text{s}^{-1}$			

At lower fluence levels (between 0.61 and $1.55 \text{ J}\cdot\text{cm}^{-1}$) and low scan speed ($5 \text{ mm}\cdot\text{s}^{-1}$) piezoelectric substrates are partially fluidized and a small part of fluidized material is vaporized. A higher scan speed results in a larger amount of ablation. Under high fluence ($3.1 \text{ J}\cdot\text{cm}^{-1}$) and high scan speed ($20 \text{ mm}\cdot\text{s}^{-1}$), the thermal energy is quickly absorbed in the region directly struck by the laser beam, and it also slowly transfers to the surroundings due to the low conductivity of ceramic materials. As a result, the central region has a higher temperature than the adjacent regions. The central region that

accumulates more energy is sputtered sooner than the adjacent regions, which results in a V-shaped profile since the central region is always ablated first. In contrast, at low scan speed and lower fluences (0.61 and $1.55 \text{ J}\cdot\text{cm}^{-2}$), the energy accumulates faster and a smaller amount of fluidized substrate is vaporized. Thus, materials are etched more evenly along the periphery of the structure, resulting in a U-shaped profile. Table 3 clearly notes the profile change from U-shaped to V-shaped as the fluence increases from 1.55 to $3.1 \text{ J}\cdot\text{cm}^{-2}$.

4. Conclusions

A study using a picosecond UV laser to machine microstructures in piezoelectric substrates is presented. The study is focused on AT-cut quartz, Lithium Niobate (LiNbO_3) and Lithium Tantalate (LiTaO_3). The experimental study examines the ablation rates while varying several major operating parameters. Linear relationships have been identified between the ablation depth and the scan number. A similar relationship is also observed between the ablation depth and pulse fluence. Results have indicated that for LiNbO_3 and LiTaO_3 the surface roughness (500 nm) of ablated surfaces does not change with the scan speeds higher than $20 \text{ mm}\cdot\text{s}^{-1}$, while for the AT-cut quartz the best roughness (550 nm) is obtained at low speed (less than $10 \text{ mm}\cdot\text{s}^{-1}$); also, increasing fluence increases the surface roughness and the resulting debris are hard to remove. The best fluence is observed at $1.5 \text{ J}\cdot\text{cm}^{-1}$ independently of the materials. It's also found in the present study that ablation at a relatively high fluence ($1.55 \text{ J}\cdot\text{cm}^{-2}$ and $3.1 \text{ J}\cdot\text{cm}^{-2}$) tends to form a U-shaped profile for AT-cut quartz at low scan speed ($5 \text{ mm}\cdot\text{s}^{-1}$), while an oval shaped. V-shaped is observed at high scan speed ($20 \text{ mm}\cdot\text{s}^{-1}$). Concerning LiNbO_3 and LiTaO_3 , the U-shaped is also observed for low scan speed ($5 \text{ mm}\cdot\text{s}^{-1}$) and at a fluence equal to $1.55 \text{ J}\cdot\text{cm}^{-2}$. For high fluence (between 2.45 and $3.1 \text{ J}\cdot\text{cm}^{-2}$) inhomogeneous shape is observed. The V-shaped is observed for both materials for high scan speed ($20 \text{ mm}\cdot\text{s}^{-1}$) at high fluence.

The present study indicates that picosecond laser can be used to micromachine materials with low thermal conductivity and high melting temperature. According to results obtained, further development in ablating non-conventional materials should be encouraged.

Acknowledgments

ERDF—Wallonia co-funded project MINATIS and WBHealth project BIOBACTIL (No. 1318026).

Author Contributions

Lamia EL Fissi and Victor Xhurdebise planned and performed the reported experiments and their analysis. Laurent A. Francis has lead the research and promoted the idea of laser etching piezoelectric substrates. Lamia EL Fissi has written the main manuscript and prepared the figures and tables. All authors reviewed the manuscript.

Conflicts of Interest

The authors declare no conflict of interest.

References

- 1 Christensena, F.K.; Mullenborn, M. Sub-band-gap laser micromachining of lithium niobate. *Appl. Phys. Lett.* **1995**, *66*, 2772–2773
- 2 Ashby, C.I.H.; Brannon, P.J. Laser-driven chemical reaction for etching LiNbO₃. *Appl. Phys. Lett.* **1986**, *49*, 475–477.
- 3 Eyett, M.; Bauerle, D. Influence of the beam spot size on ablation rates in pulsed-laser processing. *Appl. Phys. Lett.* **1987**, *51*, 2054–2055.
- 4 Ready, J.F.; Farson, D. *LIA Handbook of Laser Material Processing*; Laser Institute of America: Orlando, FL, USA, 2001.
- 5 Gower, M.C.; Crafer, R.C.; Oakley, P.J. *Laser Processing in Manufacturing*; Chapman and Hall: London, UK, 1993.
- 6 Gattass, R.; Mazur, E. Femtosecond laser micromachining in transparent materials. *Nat. Photonics* **2008**, *2*, 219–225.
- 7 Lim, D.; Kamotani, Y.; Cho, B.; Mazumder, J.; Takayama, S. Fabrication of microfluidic mixer and artificial vasculatures using a high-brightness diode-pumped Nd:YAG laser direct write method. *Lab Chip* **2003**, *3*, 318–323.
- 8 Dauer, S.; Ehlert, A.; Büttgenbach, S. Rapid prototyping of micromechanical devices using a Q-switched Nd:YAG laser with optional frequency doubling. *Sens. Actuators A Phys.* **1999**, *76*, 381–385.
- 9 Rizvi, N.H. Femtosecond laser micromachining: Current status and applications. *RIKEN Rev.* **2003**, *50*, 107–112.
- 10 Hwang, D.J.; Choi, T.Y.; Grigoropoulos, C.P. Liquid-assisted femtosecond laser drilling of straight and three-dimensional microchannels in glass. *Appl. Phys. A* **2004**, *79*, 605–612.
- 11 Sugioka, K.; Masuda, M.; Hongo, T.; Cheng, Y.; Shihoyama, K.; Midorikawa, K. Three-dimensional microfluidic structure embedded in photostructurable glass by femtosecond laser for lab-on-chip applications. *Appl. Phys. A* **2004**, *79*, 815–817.
- 12 Giridhar, M.S.; Seong, K.; Schülzgen, A.; Khulbe, P.; Peyghambarian, N.; Mansuripur, M. Femtosecond pulsed laser micromachining of glass substrates with application to microfluidic devices. *Appl. Opt.* **2004**, *43*, 4584–4589.
- 13 Ho, H.; Aitchison, J.S.; Eaton, S.; Herman, P.R.; Li, J. F₂-laser microfabrication for integration optical circuits with microfluidic biochips. *Proc. SPIE* **2004**, *5591*, 96–103.
- 14 Klank, H.; Kutter, J.P.; Geschke, O. CO₂-laser micromachining and back-end processing for rapid production of PMMA-based microfluidic systems. *Lab Chip* **2002**, *2*, 242–246.
- 15 Ozkan, A.M.; Malshe, A.P.; Railkar, T.A.; Brown, W.D. Femtosecond laser induced periodic structure writing on diamond crystals and microclusters. *Appl. Phys. Lett.* **1999**, *75*, 3716–3718.
- 16 Will, M.; Nolte, S.; Tunnerman, A. Single and multimode waveguides in glasses manufactured with femtosecond laser pulses. *Proc. SPIE* **2002**, *4633*, 99–106.
- 17 Zhang, Y.; Lowe, R.M.; Harvey, E.; Hannaford, P.; Endo, A. High aspect-ratio micromachining of polymers with an ultrafast laser. *Appl. Surf. Sci.* **2002**, *186*, 345–351.
- 18 Pronko, P.P.; Dutta, S.K.; Squier, J.; Rudd, J.V.; Du, D.; Mourou, G. Machining of sub-micron holes using a femtosecond laser at 800 nm. *Opt. Commun.* **1995**, *114*, 106–110.

- 19 Kim, T.; Kim, H.S.; Hetterich, M.; Jones, D.; Girkin, J.M.; Bente, E.; Dawson, M.D. Femtosecond laser machining of gallium nitride. *Mater. Sci. Eng. B* **2001**, *82*, 262–264.
- 20 Zheng, H.Y.; Zareena, A.R.; Huang, H.; Lim, G.C. Studies of femtosecond laser-processed nitinol. *Mater. Sci. Forum* **2003**, *437*, 227–280.
- 21 Wellershoff, S.S.; Hohlfeld, J.; Gudde, J.; Matthias, E. The role of electron-phonon coupling in femtosecond laser damage of metals. *Appl. Phys. A* **1999**, *69*, S99–S107.
- 22 Groeneveld, R.H.M.; Sprik, R.; Lagendijk, A. Femtosecond spectroscopy of electron-electron and electron-phonon energy relaxation in Ag and Au. *Phys. Rev. B* **1995**, *17*, 11433–11445.
- 23 Chichkov, B.N.; Momma, C.; Nolte, S.; von Alvensleben, F.; Tünnermann, A. Femtosecond, picosecond and nanosecond laser ablation of solids. *Appl. Phys. A* **1996**, *63*, 109–115.
- 24 Nolte, S.; Momma, C.; Jacobs, H.; Tünnermann, A.; Chichkov, B.N.; Wellegehausen, B.; Welling, H. Ablation of metals by ultra-short laser pulses. *J. Opt. Soc. Am. B* **1997**, *14*, 2716–2722.
- 25 Breitling, D.; Ruf, A.; Dausinger, F. Fundamental aspects in machining of metals with short and ultrashort laser pulses. *Proc. SPIE* **2004**, *5339*, 49–63.
- 26 Drogoff, L.; Vidal, F.; Laville, S.; Chaker, M.; Johnston, T.; Barthelemy, O.; Margot, J.; Sabasi, M. Laser ablated volume and depth as a function of pulse duration in aluminum targets. *Appl. Opt.* **2005**, *44*, 278–281.
- 27 Quartz General Material Specification. Available online: <http://www.roditi.com/SingleCrystal/Quartz/QuartzHead.htm> (accessed on 13 March 2014).
- 28 MTI Webpage. SAW Grade LiNbO₃ Wafers. Available online: <http://www.mtixtl.com/sawgradelinbo3wafers.aspx> (accessed on 13 April 2014).
- 29 Samad, R.; Courrol, L.; Baldochi, S.; Vieira, N. Ultrashort Laser Pulses Applications. In *Coherence and Ultrashort Pulse Laser Emission*; InTech: New York, NY, USA, 2012.
- 30 Rosenfeld, A.; Lorenz, M.; Ashkenasi, D.; Stoian, R. Ultrashort-laser pulse damage threshold of transparent materials and the role of incubation. *Appl. Phys. A* **1999**, *69*, S373–S376.
- 31 Duley, W.W. *UV Lasers: Effects and Applications in Materials Science*; Cambridge University Press: New York, NY, USA, 1996.
- 32 Patzel, R. An introduction to excimer lasers. In *Photonics Handbook*, 44th ed.; Laurin Publishing: New York, NY, USA, 2002.
- 33 Micromachining of Glass Using a Fiber-Based, High Average Power Picosecond Laser. Available online: <http://www.coherent.com/download/6664&cmpid=EMC450> (accessed on 13 February 2014).
- 34 Zheng, B.; Jiang, G.; Wang, W.; Wang, K.; Mei, X. Ablation experiment and threshold calculation of titanium alloy irradiated by ultra-fast pulse laser. *AIP Adv.* **2014**, *4*, 031310.
- 35 Gamaly, E.G.; Rodea, A.V.; Uteza, O.; Samoc, M.; Luther-Davies, B. Transient reflectivity of gallium films induced by femtosecond laser. *Appl. Surf. Sci.* **2002**, *197*, 730–736.
- 36 Rubahn, H.G. *Laser Applications in Surface Science and Technology*; Wiley: New York, NY, USA, 1999.